

Complex phases in the doped two-species bosonic Hubbard Model

Kalani Hettiarachchilage,¹ Valéry G. Rousseau,¹ Ka-Ming Tam,^{1,2} Mark Jarrell,^{1,2} and Juana Moreno^{1,2}

¹*Department of Physics and Astronomy, Louisiana State University, Baton Rouge, Louisiana 70803, USA*

²*Center for Computation and Technology, Louisiana State University, Baton Rouge, LA 70803, USA*

(Dated: December 19, 2012)

We study a two-dimensional bosonic Hubbard model with two hard-core species away from half filling using Quantum Monte Carlo simulations. The model includes a repulsive interspecies interaction and different nearest-neighbor hopping terms for the two species. By varying the filling we find a total of five distinct phases, including a normal liquid phase at higher temperature, and four different phases at lower temperature. We find an anti-ferromagnetically ordered Mott insulator and a region of coexistent anti-ferromagnetic and superfluid phases near half filling. Further away from half filling the phase diagram displays a superfluid phase and a novel phase inside the superfluid region at even lower temperatures. In this novel phase separated region, the heavy species has a Mott behavior with integer filling, while the lighter species shows phase separated Mott and superfluid behaviors.

PACS numbers: 02.70.Uu, 05.30.Jp

A major undertake in condensed matter physics is the study of exotic quantum phases. Strongly correlated systems display quantum criticality, coexistent and inhomogeneous phases, and secondary ordered phases close to quantum critical points.¹ These exotic phenomena occur due to competing complex interactions of spin, charge, lattice, and orbital character. Competing phases in strongly correlated electronic systems² occur in ruthenates,³ manganites,⁴ cuprates,⁵ cobalt oxides,⁶ organic salts⁷ and heavy fermion materials.⁸ Since competing phases can be tuned via external parameters, there are exciting opportunities for advance device applications of complex materials.

Cold atoms experiments⁹ have become a playground for realizations of the Hubbard^{10,11} and other strongly correlated model Hamiltonians, since model parameters can be tuned using laser and magnetic fields.^{12,13} Recently, there is an increasing interest in studies of mixtures of atoms due to the complexity associated with multiple species and the possibility of discovering novel phases. These include mixtures of bosonic and fermionic atoms¹⁴ and mixtures of two different bosonic species.¹⁵ Moreover, the experimental study of the ⁸⁴Rb-⁴¹K bosonic mixture in a three dimensional optical lattice¹⁶ has motivated theoretical studies of the half-filled Hubbard model with two species with different masses or hopping integrals.^{17,18} These studies reveal a rich phase diagram. The concentration of carriers may also be controlled in experiments, which motivated our study.

We consider two species of hard-core bosons a and b confined to a two-dimensional lattice. The Hamiltonian takes the form:

$$\hat{\mathcal{H}} = -t_a \sum_{\langle i,j \rangle} \left(a_i^\dagger a_j + H.c. \right) - t_b \sum_{\langle i,j \rangle} \left(b_i^\dagger b_j + H.c. \right) + U^{ab} \sum_i \hat{n}_i^a \hat{n}_i^b \quad (1)$$

where a_i^\dagger (b_i^\dagger) and a_i (b_i) are the creation and annihilation operators, respectively, of hard-core bosons a (b), and $\hat{n}_i^a = a_i^\dagger a_i$, $\hat{n}_i^b = b_i^\dagger b_i$ are the number operators of a , b bosons on site i , respectively. The sum $\sum_{\langle i,j \rangle}$ runs over all distinct pairs of first neighboring sites i and j , t_a (t_b) is the hopping integral between i and j sites for species a (b), and U^{ab} is the strength of the interspecies repulsion. Since we are in the hard-core limit, creation and annihilation operators satisfy commutation rules on different sites $i \neq j$, $[a_i, a_j] = [a_i^\dagger, a_j^\dagger] = [a_i, a_j^\dagger] = 0$, and anti-commutation rules on identical sites, $\{a_i^\dagger, a_i^\dagger\} = \{a_i, a_i\} = 0$ and $\{a_i, a_i^\dagger\} = 1$.

We perform Quantum Monte Carlo simulations using the Stochastic Green Function algorithm¹⁹ with Global Space-Time Updates²⁰ for the canonical ensemble on $L \times L$ lattices with an inverse temperature $\beta = 8L$. Our results at half-filling reproduce the phase diagram of Ref. 18. We focus on the unpolarized phase diagram, so our total density is $\rho = N/L$ with $N = N_a + N_b = 2N_a$, with N_a and N_b the number of a and b particles, respectively. Since our intention is to explore the doping dependence of the model we restrict our simulation to the following parameters: $t_a = 0.08t$, $t_b = t$, and $U^{ab} = 6t$, where $t = 1$.

In Fig. 1 we look for signatures of ordering. To look for phase separation and Mott states, we calculate the chemical potential by adding one a and one b particle to the system as $\mu = (E(N+2) - E(N))/2$. The superfluid (SF) phase is detected by measuring the superfluid density, ρ_{SF} , using the fluctuations of the winding number, W , via Pollock and Ceperley's formula²¹. The antiferromagnetic (AF) phase is characterized by a finite density-density static structure factor: $S(\hat{k}) = \frac{1}{L^2} \sum_{\hat{p}, \hat{q}} \exp[i\hat{k} \cdot (\hat{p} - \hat{q})] \langle n_{\hat{p}}^{(a,b)} n_{\hat{q}}^{(a,b)} \rangle$. We find an AF phase at half filling $\rho_1 = 1$. It is characterized by a vanishing compressibility, $\kappa = \partial\rho/\partial\mu$ (top panel), a finite static staggered structure factor (bottom panel), as well as AF

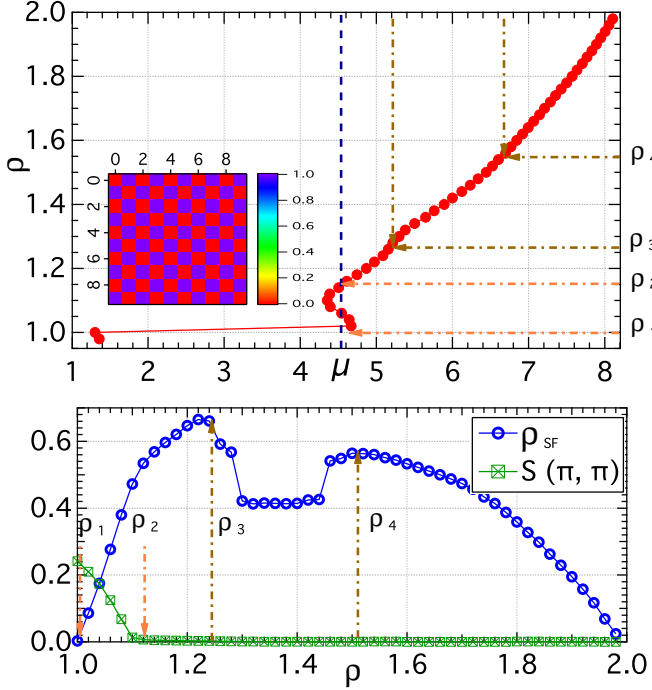


FIG. 1: (Color online) Top panel: The average density, $\rho = N/L$ as a function of the chemical potential, μ . The vertical blue dashed line shows the Maxwell construction between ρ_1 and ρ_2 . The brown dotted-dashed lines show different phase boundaries at ρ_3 and ρ_4 as discussed in the text. The inset shows a snapshot of the density profile at half filling, $\rho = \rho_1 = 1$, with the blue (red) squares indicating $n_i^b = 1$ ($n_i^a = 1$). Bottom panel: The superfluid density (blue circles) and the staggered structure factor (green squares) as a function of ρ . The dot-dashed lines show different phase boundaries. All data are for $L = 10$, $\beta = 80$, $t_a = 0.08$, $t_b = 1.00$ and $U^{ab} = 6$. Error bars are smaller than symbol sizes.

ordering as shown in a snapshot of the density profile (inset of the top panel). Near half filling, $\rho = N/L$ vs. μ displays a first-order phase transition between ρ_1 and $\rho_2 \sim 1.16$ with instability, characterized by a negative slope, in a portion of the region. These two phases with densities ρ_1 and ρ_2 coexist for any density value between the two end points. Since, in this region the system displays finite values of $S(\pi, \pi)$ and ρ_{SF} we conclude that AF and SF phases coexist for any $\rho_1 < \rho < \rho_2$. A homogeneous SF state exists between ρ_2 and $\rho_3 \sim 1.25$ identified by measuring the superfluid density ρ_{SF} . At ρ_3 the superfluid density displays a decrease and the ρ versus μ plot shows a small bump. Another small feature is displayed in the top panel at $\rho_4 \sim 1.52$. Finally, the homogeneous SF phase continues until full filling. Next, we investigate the unexpected lowering of the superfluid density between ρ_3 and ρ_4 .

Fig. 2 shows snapshots of the average local density of both species for $\rho_3 < \rho = 1.44 < \rho_4$. Simulations with open and periodic boundary conditions show clear evidence of phase separation. Species a always shows Mott

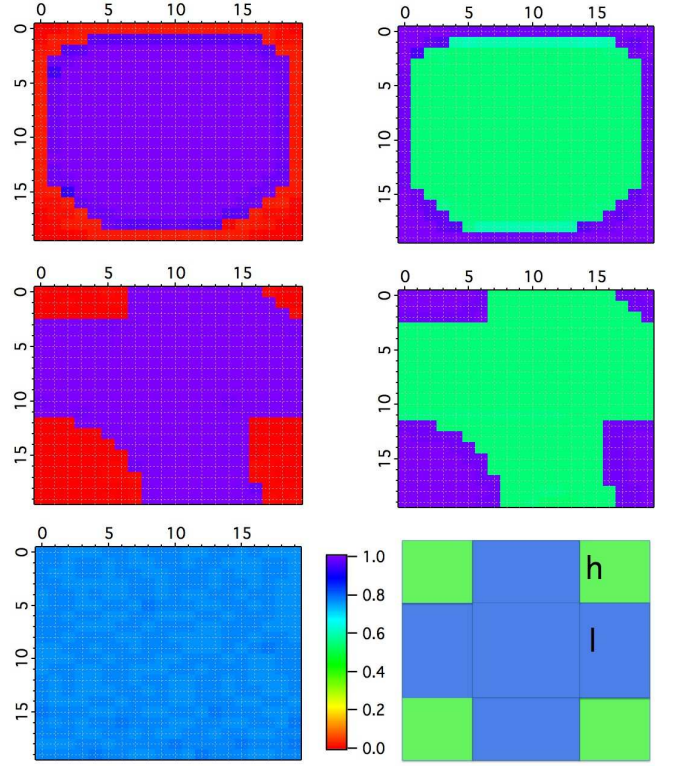


FIG. 2: (Color online) Snapshot of the average local density of a and b particles for $L = 20$ and $\rho = 1.44$. Top panel: Open boundary conditions. The a and b local densities, $\langle n_i^a \rangle$ and $\langle n_i^b \rangle$, are shown on the left and right panels, respectively. For a particles, sites close to the boundary (red) have $\langle n_i^a \rangle \sim 0$, while the occupation of the central (blue) region is $\langle n_i^a \rangle \sim 1$. For b particles (right panel) the density close to the boundary (blue region) is $\langle n_i^b \rangle \sim 1$, and at the center (green region), $\langle n_i^b \rangle \sim 0.60$. Middle panel: The same quantities shown in the top panel but with periodic boundary conditions. Bottom panel: At the left the homogeneous density distribution of both a and b particles for $\rho = 1.72$. At the right, a sketch of the density profile for a simulation with periodic boundary conditions.

behavior with $\langle n_i^a \rangle \sim 0$ or 1, while species b displays Mott $\langle n_i^b \rangle \sim 1$ and SF coexistent phases. We can understand the tendency of the system to form such a mixed phase by extending the bosonic mean-field formalism^{10,22} to two-species bosons in the hardcore limit.¹⁷ Using the Gutzwiller variational approach,²³ the most general site factorized wave function can be written as

$$\Psi = \prod_i \Psi_i = \prod_i \left[\sin \frac{\theta}{2} \left(\sin \frac{\alpha}{2} a_i^\dagger + \cos \frac{\alpha}{2} b_i^\dagger \right) + \cos \frac{\theta}{2} \left(\sin \frac{\beta}{2} + \cos \frac{\beta}{2} a_i^\dagger b_i^\dagger \right) \right] |0\rangle, \quad (2)$$

where θ , α and β are variational parameters and $|0\rangle$ is the vacuum state. The energy function per lattice site

takes the form

$$\frac{E}{L^2} = -t_a \sin^2 \theta \cos^2 \left(\frac{\alpha - \beta}{2} \right) - t_b \sin^2 \theta \sin^2 \left(\frac{\alpha + \beta}{2} \right) + U^{ab} \cos^2 \frac{\theta}{2} \cos^2 \frac{\beta}{2}. \quad (3)$$

We minimize E subject to constraints on the densities: $n_a = \frac{N_a}{L^2} = \sum_i \frac{\langle \Psi | n_i^a | \Psi \rangle}{L^2}$ and $n_b = \frac{N_b}{L^2} = \sum_i \frac{\langle \Psi | n_i^b | \Psi \rangle}{L^2}$.

We solve these nonlinear equations by constructing an error function and minimizing it. For $\rho = 1.44$, within this approximation, we find that the phase separated state is lower in energy than an homogeneous superfluid phase. The total energy of a superfluid with homogeneous densities $\rho_a = \rho_b = 0.72$ is 804.33 for $L = 20$. The bottom right panel of Fig. 2 represents the phase separated state as a central cross with area $(2h + l)^2 - 4h^2$ and four corner squares of area h^2 . If we assume that in the cross $n_i^a = 1.0$ and $n_i^b = 0.60$ for all i sites the mean-field energy is 754.19. At the four squares $n_i^a = 0.0$ and $n_i^b = 1.0$ and the total energy is zero since it is a Mott state. We can hypothesis that this new PS region becomes stable to reduce the potential energy. Consequently there is a critical U_c^{ab} above which the phase separated state is stable. We estimate $U_c^{ab} \sim 4.8$ for our chosen parameters, $t_a = 0.08$, $t_b = 1.0$ and $\rho = 1.44$.

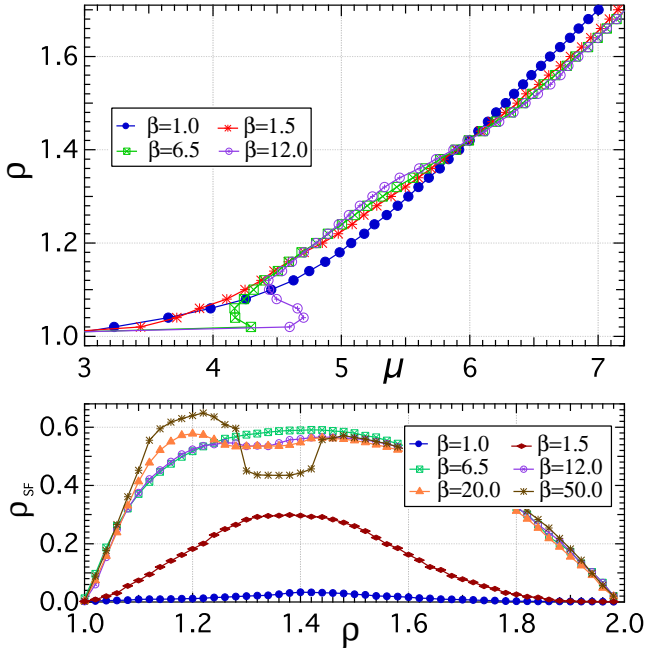


FIG. 3: (Color online) Top panel: Average density, ρ , versus chemical potential, μ , for different temperatures. Bottom panel: The superfluid density, ρ_{SF} , as a function of ρ for different temperatures. All data are for system size $L = 10$. Error bars are smaller than symbol sizes.

Next we study the temperature dependence of ρ and ρ_{SF} . The top panel of Fig. 3 shows ρ versus μ for a system

of size $L = 10$ and different inverse temperatures. Since there is a clear signature of phase separation for $\beta = 6.5$ but not for $\beta = 1.5$, we can conclude that the critical AF temperature occurs between these two temperatures. Similarly, from the ρ_{SF} vs. ρ curves for different temperatures (see bottom panel of Fig. 3), we can conclude that for this cluster size the phase separated region between ρ_3 and ρ_4 appears for temperatures between $\beta = 6.5$ and $\beta = 12$. We infer the phase diagram by appropriate scaling of our finite-size results.

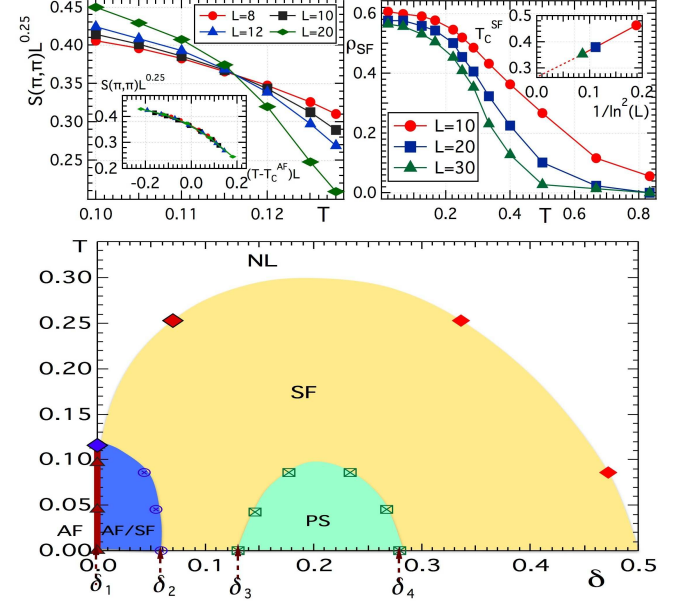


FIG. 4: (Color online) Bottom panel: The temperature, T , versus doping, δ , phase diagram with equal population of each species. At half-filling, the system is antiferromagnetic (AF) below $T_c^{AF} \sim 0.116$ and normal liquid (NL) at larger temperatures. By increasing the doping a discontinuous transition from AF to superfluid (SF) phase occurs, and an AF/SF phase separated region develops between $\delta_1 = 0$ and $\delta_2 = 0.06$. Between $\delta_3 = 0.13$ and $\delta_4 = 0.28$ phase separation (PS) occurs with the heavy species becoming Mott while the lighter one displays regions with either Mott or superfluid behaviors. Top left panel: Scaling behavior of the static staggered structure factor for the continuous transition from AF to NL at half filling, $\delta_1 = 0$ (corresponds to the filled blue diamond in the bottom panel). Inset shows the collapse near to critical temperature with the Ising-like critical exponents. Top right panel: Superfluid density as a function of temperature for different system sizes at $\delta = 0.07$ (filled red diamond). Inset shows the finite size scaling to find the SF critical temperature in the thermodynamic limit for the continuous transition at $\delta = 0.07$. Data points are based on simulation results, lines are guides to the eye.

Fig. 4 displays the temperature, T , vs. doping, $\delta = \frac{N_a + N_b}{2L^2} - \frac{1}{2}$, phase diagram. In the thermodynamic limit, the AF phase only exists at half filling $\delta_1 = 0$ and very low temperatures. The top left panel shows

the scaling of the AF to normal liquid (NL) continuous phase transition at $\delta_1 = 0$. This transition belongs to the two-dimensional Ising universality class for which the static staggered structure factor scales as $S(\pi, \pi) = L^{-(2\beta/\nu)} f((T - T_c^{AF})L^{1/\nu})$, where f is a universal scaling function, and β and ν are the critical exponents for the order parameter and the correlation length, respectively. The factor $2\beta/\nu = 1/4$ in two-dimensional systems. Therefore we can read the critical temperature at the point where the $S(\pi, \pi)L^{1/4}$ vs. T curves for different system sizes cross. For our parameters $T_c^{AF} = 0.116$, and $S(\pi, \pi)L^{1/4}$ vs. $(T - T_c^{AF})L$ curves collapse. The AF phase is represented by a red line ending on a blue diamond in Fig. 4. As we illustrate in previous figures, near half filling, we find a discontinuous transition from AF to SF phase and a phase separation region for doping $\delta_1 = 0.0 \lesssim \delta \lesssim \delta_2 = 0.06$ (dark blue region in Fig. 4). The boundary of the AF/SF phase separated region is found by a Maxwell's construction of the ρ vs. μ plots. The PS region inside the SF phase exists for $\delta_3 = 0.13 \lesssim \delta \lesssim \delta_4 = 0.28$. For a given temperature we determine its boundaries by estimating the filling where ρ_{SF} starts decreasing (ρ_3 in Fig. 1) or stop increasing (ρ_4). For the rest of dopings we encounter a SF phase at low temperatures and an NL at higher temperatures. The top right panel of Fig. 4 shows the superfluid density as a function of temperature for different system sizes. The order parameter, superfluid density, has the universal jump of $\frac{\rho_{SF}}{T} = \frac{2}{\pi}$ at the critical point.²⁴ The transition from SF to NL is continuous and belongs to the Kosterlitz Thouless universality class. We find T_c in the thermodynamic limit by using the relation between the size dependent critical temperature $T_c(L)$ and the cluster size: $T_c(L) - T_c(\infty) \propto \frac{1}{\ln^2(L)}$.²⁵ The inset on the right top panel displays this scaling. For $\delta = 0.07$ ($\rho = 1.14$) we find $T_c = 0.254$. Scaled transition points are shown as red diamonds in Fig. 4. There is one triple point where AF, SF and NL phases coexist.

In summary, by changing doping we find complex phases in the two-dimensional two-species hardcore bosonic Hubbard model for equal populations and unequal hopping. We find a first order phase transition between the AF phase at half filling and a SF phase near half filling with a region of SF and AF coexistence. For a broad region of fillings and temperatures away from half filling, a SF phase is found. However, within the SF phase at finite doping we find a dome-shaped region containing an inhomogeneous phase. Density profiles of this novel phase separated region show that the heavier species displays Mott insulating behavior, while the lighter species is phase separated in Mott and superfluid regions. Farther from half filling, both species display an homogeneous superfluid phase. This complex phase diagram reminds us about the phase diagram of cuprates. In particular, our phase diagram displays a region that is similar to the so-called “superconducting dome” away from half-filling. Further, we believe our work will encourage experimental studies of this model on cold atoms traps. Indeed the experimental realization of half-filling AF phase is hard due to the low entropy associated with this phase, while the complex mixed phase that we identify away from half-filling can be expected to have a high entropy and, then, be easier to obtain. To further explore this complex phase diagram we are planning to extend our simulations to polarized systems with different species population.

We would like to thank Dana Browne and Dimitrios Galanakis for useful discussions. This work is supported by NSF OISE-0952300 (KH, VGR and JM) and by DOE SciDAC grant DE-FC02-06ER25792 (KMT and MJ). This work used the Extreme Science and Engineering Discovery Environment (XSEDE), which is supported by the National Science Foundation grant number DMR100007, and the high performance computational resources provided by the Louisiana Optical Network Initiative (<http://www.loni.org>).

-
- ¹ S. Yunoki, *et al.*, Phys. Rev. Lett. **80**, 845 (1998); A. Moreo, *et al.*, Science, **283**, 2034 (1999); V. Kiryukhin, *et al.*, Phys. Rev. B **63**, 024420 (2000); M. Uehara, *et al.*, Nature **399**, 560 (1999); E. Dagotto, *et al.*, Phys. Rep. **344**, 1 (2001); P. Coleman and A. J. Schfield, Nature, **433**, 227 (2005); Q. Si and F. Steglich, Science, **329**, 1161 (2010).
- ² E. Dagotto, Science, **309**, 257 (2005).
- ³ S. Nakatsuji, *et al.*, Phys. Rev. Lett. **93**, 146401 (2004).
- ⁴ J. F. Mitchell, *et al.*, J. Phys. Chem. B **105**, 10731 (2001).
- ⁵ M. Vershinin, *et al.*, Science **303**, 1995 (2004).
- ⁶ M. L. Foo, *et al.*, Phys. Rev. Lett. **92**, 247001 (2004).
- ⁷ P. Limelette, *et al.*, Phys. Rev. Lett. **91**, 016401 (2003).
- ⁸ V. A. Sidorov, *et al.*, Phys. Rev. Lett. **89**, 157004 (2002); A. R. Schmidt, *et al.*, Nature, **465**, 7298, (2010).
- ⁹ M. Greiner, *et al.*, Nature, **415**, 39 (2002).
- ¹⁰ M. P. A. Fisher, *et al.*, Phys. Rev. B **40**, 546 (1989).
- ¹¹ G. G. Batrouni and R. T. Scalettar, Phys. Rev. Lett. **84**, 1599 (2000).
- ¹² E. Timmermans, *et al.*, Phys. Rep. **315**, 199, (1999).
- ¹³ T. Köhler, *et al.*, Rev. Mod. Phys. **78**, 1311, (2006).
- ¹⁴ F. Schreck, *et al.*, Phys. Rev. Lett. **87**, 080403 (2001); A. Albus, *et al.*, Phys. Rev. A **68**, 023606 (2003); G. Modugno, *et al.*, Science, **297** (2002); C. Ospelkaus, *et al.*, Phys. Rev. Lett. **96**, 020401 (2006).
- ¹⁵ G. Roati, *et al.*, Phys. Rev. Lett. **99**, 010403 (2007); G. Thalhammer, *et al.*, Phys. Rev. Lett. **100**, 210402 (2008); S. B. Papp, *et al.*, Phys. Rev. Lett. **101**, 040402 (2008).
- ¹⁶ J. Catani, *et al.*, Phys. Rev. A **77**, 011603 (2008).
- ¹⁷ E. Altman, *et al.*, New J. Phys. **5**, 113 (2003).
- ¹⁸ S. G. Söyler, *et al.*, New J. Phys. **11**, 073036 (2009); B. Capogrosso-Sansone, *et al.*, Phys. Rev. A **81**, 053622 (2010).

- ¹⁹ V.G. Rousseau, Phys. Rev. E **77**, 056705 (2008); V. G. Rousseau, Phys. Rev. E **78**, 056707 (2008).
- ²⁰ V.G. Rousseau and D. Galanakis, arXiv:1209.0946 (2012).
- ²¹ E. L. Pollock and D. M. Ceperley, Phys. Rev. B **36**, 8343 (1987).
- ²² K. Sheshadri, *et al.*, Europhys. Lett. **22**, 257 (1993).
- ²³ D. S. Rokhsar and B. G. Kotliar, Phys. Rev. B **44**, 10328 (1991).
- ²⁴ D. R. Nelson and J. M. Kosterlitz, Phys. Rev. Lett. **39**, 1201 (1977).
- ²⁵ M. Boninsegni, and N. Prokof'ev, Phys. Rev. Lett. **95**, 237204 (2005).